











# Experimental Analysis of the Spectral Reflectivity of Metallic Blazed Diffraction Gratings in the THz Range for Space Instrumentation

Gonzalo García-Lozano , Guillermo Mercant , Marianela Fernández-Rodríguez , María Carmen Torquemada , Luis M. González , Tomás Belenguer , Alexander Cuadrado , Luis Miguel Sánchez-Brea , Javier Alda , and Mahmoud Elshorbagy 

**Abstract**—The core of spectrometers for deep space exploration in the far-infrared spectral range is a diffraction grating optimized for a defined range of wavelengths. This contribution presents an in-depth analysis of the fabrication, morphological characterization, and spectral efficiency verification of this type of gratings operating in the THz range. Two different manufacturing techniques were used: the first one was laser ablation and microstructuring with a five-axis femtosecond laser system, and the second one was a traditional micromachining technique using milling tools. The gratings have a blazed geometry with saw-tooth profiles that enhances the efficiency of the diffracted order of interest,  $m = 1$ , at the TM polarization mode, and within a spectral range between 70 and 114  $\mu\text{m}$ . The morphological features of the fabricated gratings were measured by confocal microscopy and analyzed using topographic parameters. The measured averaged profiles were used to compute the diffraction efficiency of the fabricated gratings and to compare the actual manufactured profiles against the experimental results. Our measurement setup fixes the wavelength of the illuminating source to six values between 60 and 120  $\mu\text{m}$  (2.5 and 4.7 THz). At each of these spectral lines, we have scanned the angle of incidence between 20° and 75°. This angular range includes the nominal value of the angle of incidence,  $\theta_{\text{inc}} = 57^\circ$ . The experimental

values of efficiency can be easily compared with those resulting from computation, where the efficiency is calculated for each one of the available wavelengths as a function of the angle of incidence. This approach has allowed us to validate the design and conclude that gratings fabricated using femtosecond laser ablation perform better than those obtained through micromachining processes. In any case, both manufacturing techniques generate gratings above the validation threshold for diffraction efficiency,  $\eta > 0.65$ .

**Index Terms**—Computational electromagnetism, diffraction efficiency, diffraction gratings, far-IR optics, terahertz (THz) optics.

## I. INTRODUCTION

ADVANCES in cosmology and astrophysics research imply the efficient detection of electromagnetic radiation in the terahertz (THz) range. Radiation from space provides relevant information about distant galaxies and the birth and evolution of stars and planetary systems. Half of the energy produced by star-forming activity is emitted through the infrared part of the spectrum (8–1000  $\mu\text{m}$ ) [1], [2]. The longer the wavelength of the radiation analyzed, the further away it comes from. In addition, it is believed that a significant amount of carbon in space exists as large molecules known as polycyclic aromatic hydrocarbons, although they have not been directly observed [3]. These compounds have far-infrared (FIR) vibrational transitions whose detection would contribute to the better knowledge of the chemistry in the formation of stars and planets. Factors, such as the atmosphere opacity of the Earth force these observations to be carried out on space missions.

So, a future observatory would be a large space telescope including a FIR spectrometer. In the THz radiation range, from 30–100 microns, the development of high-performance instrumentation presents a challenge, as those already evaluated in the Space Infrared telescope for Cosmology and Astrophysics (SPICA) mission proposal, that already incorporated a FIR spectrometer, Spica far-infrared instrument (SAFARI) [4]. The received radiation had to be directed toward a spectrometer composed of four modules, each operating in a different range of wavelengths. Some of the authors have been in charge of the development of the spectrometer module [5] operating in the 70–114  $\mu\text{m}$  range (2.6–4 THz). Although the mission was canceled due to technological immaturity, astronomers have not

Received 3 July 2024; revised 24 September 2024; accepted 29 October 2024. Date of publication 7 November 2024; date of current version 8 January 2025. The work of Gonzalo García-Lozano, Guillermo Mercant, M. Fernández, M. Carmen Torquemada, Luis M. González, and Tomás Belenguer was supported by the project PID2022-142490OB-C33 funded by MCIN/AEI /10.13039/501100011033/ and by FEDER “Una manera de hacer Europa”. The work of Javier Alda and Luis Miguel Sánchez-Brea was supported by Plan Nacional de Investigación of the Ministerio de Ciencia e Innovación “VDOEST” project PID2022-138071OB-I00. The work of Alexander Cuadrado was supported by the program Proyectos de I+D para jóvenes investigadores de la Universidad Rey Juan Carlos financiado por la Comunidad de Madrid, Código 2022/00156/025, REF:M2742. (Corresponding author: Gonzalo García-Lozano.)

Gonzalo García-Lozano, Guillermo Mercant, Marianela Fernández-Rodríguez, María Carmen Torquemada, Luis M. González, and Tomás Belenguer are with the Departamento de Óptica Espacial, Instituto Nacional de Técnica Aeroespacial (INTA), 28850 Madrid, Spain (e-mail: ggarloz@inta.es).

Alexander Cuadrado is with the Escuela de Ciencias Experimentales y Tecnología, Universidad Rey Juan Carlos, 28933 Madrid, Spain.

Luis Miguel Sánchez-Brea is with the Facultad de Ciencias Físicas, Universidad Complutense de Madrid, 28040 Madrid, Spain.

Javier Alda is with the Facultad de Óptica y Optometría, Universidad Complutense de Madrid, 28037 Madrid, Spain.

Mahmoud Elshorbagy is with the Facultad de Óptica y Optometría, Universidad Complutense de Madrid, 28037 Madrid, Spain, and also with the Physics Department, Faculty of Science, Minia University, El Minia 61519, Egypt.

Color versions of one or more figures in this article are available at <https://doi.org/10.1109/TTHZ.2024.3493001>.

Digital Object Identifier 10.1109/TTHZ.2024.3493001

ceased their interest in analyzing radiation at these wavelengths, suggesting the implementation of FIR spectrometers in the future space missions [6], [7], [8].

This is why advances in the design and fabrication of diffraction gratings in the THz range are key preparing the technology for new challenges when they come.

The typical design for a space spectrometer is made around customized diffraction gratings. These gratings diffract radiation toward a given angular direction depending on the wavelength and some other geometrical parameters. The ratio between the period and the wavelength determines the number of available diffraction orders. In our case, the grating has a period with dimensions in the same range as the wavelength of the incoming radiation, becoming a subwavelength grating for a portion of the spectral range of interest [9]. Consequently, the grating operates with only one diffraction order, apart from the zero order. Blazed diffraction grating profiles are typically chosen to diffract most of the incident energy into the desired diffraction order. Then, the detailed design of a grating for space instrumentation depends on many factors. Some are optical, like the resolution, efficiency, and spectral range, but others are related to the demanding space conditions: vibrations, vacuum, and temperature. In fact, in the THz range, the spectral instrument must be cooled to 4K to mitigate self-emission concerning the sky background signal. A detailed analysis of the design constraints of this type of gratings has already been made [10]. Computational electromagnetism tools demonstrated their relevant role in evaluating the efficiency of the designed grating in terms of its characteristic parameters. This analysis seems mandatory when involving subwavelength gratings, as the one treated in this contribution. Rigorous coupled-wave analysis [11] and finite element method [12] (FEM) were used, looking for a design that maximizes the efficiency in the whole spectral range. This numerical analysis may also consider departures from the ideal geometry and conditions that could produce a degradation in the nominal performance of the element. Even though computational electromagnetism is a reliable tool for optimizing and analyzing the response of blazed THz gratings, experimental measurements are essential to demonstrate and verify the performance parameters of the fabricated gratings. Therefore, after Section II, we focus on the experimental validation of our designs, measuring the diffraction efficiency and comparing it with the results derived from simulation. The rest of this article is organized as follows: In Section II, we present the fundamentals of blazed gratings applicable to our case. In Section III, we analyze the morphological parameters for the gratings fabricated using two technologies: 1) laser ablation; and 2) micromachined. Here, we have obtained the mean and standard deviation of the fabricated topography and we have compared it with the nominal one. The measurements have been made using confocal microscopy across selected regions, evenly distributed on the surface of the grating to have a better idea of the homogeneity of the manufacturing process on the whole  $5 \times 4 \text{ cm}^2$  fabricated area. Section IV presents the experimental measurement of the diffraction efficiency for six available wavelengths and a quite wide range in the angle of incidence. The results obtained from the experiment are compared to those obtained from simulations

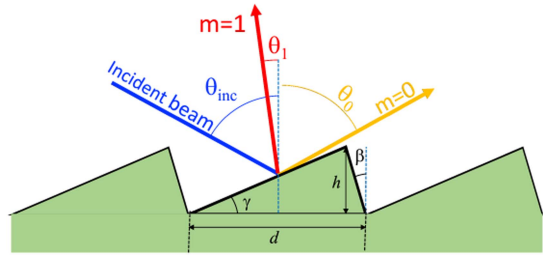


Fig. 1. Metallic grating has a period  $d$ , a height  $h$ , and a triangular profile characterized by the blaze angle  $\gamma$ , and the slant angle  $\beta$ . The incident beam subtends an angle  $\theta_{\text{inc}}$  with respect to the normal to the grating plane (horizontal). The orders of diffraction reflect with an angle given by (1). In this figure, we have followed the sign convention of the geometrical optics, meaning that  $\theta_{\text{inc}}$ , and  $\theta_1$  are positive, meanwhile,  $\theta_0$  is negative. Angles  $\gamma$  and  $\beta$  are considered positive.

TABLE I  
INITIAL REQUIREMENTS AND MORPHOLOGICAL PARAMETERS OF THE  
DESIGNED DIFFRACTION GRATING

Variable	Value
Spectral range	[70 - 114] $\mu\text{m}$
Diffraction order, $m$	1
Polarization	Transversal Magnetic (TM)
Total diffraction angle, $\Delta\theta_m$	$30^\circ - 40^\circ$
Diffraction efficiency, $\eta$	$> 65\%$
Angle of incidence, $\theta_{\text{inc}}$	$57^\circ$
Spectral resolution ( $\lambda/\Delta\lambda$ )	200
Grating period, $d$	76 $\mu\text{m}$
Blaze angle, $\gamma$	$23.5^\circ$
Slant angle, $\beta$	$10^\circ$
Height, $h$	30.7 $\mu\text{m}$

when considering the actual fabricated profile. At this point, we could see that the element fabricated using laser ablation outperforms the micromachined grating. In any case, both fabricated gratings behave above performance for the nominal operation conditions. Finally, Section V concludes this article.

## II. FUNDAMENTALS

The dispersive properties of a diffraction grating are governed by the well-known grating equation

$$d(\sin \theta_{\text{inc}} + \sin \theta_m) = m\lambda \quad (1)$$

where  $d$  is the grating period,  $\lambda$  is the wavelength, and  $m$  is the diffractive order that appears at  $\theta_m$  when the angle of incidence is  $\theta_{\text{inc}}$ . These angles are referenced relative to the line perpendicular to the diffraction grating's surface. Blazed gratings add a couple of new angles,  $\gamma$  and  $\beta$  (blaze and slant angles, respectively), that describe the geometry of a saw-tooth profile (see Fig. 1) and are related to the maximum height of the profile,  $h$  [10]. Blazing enhances the irradiance diffracted at the desired order, which in our case corresponds to  $m = 1$ . The nominal parameters of our design are presented in Table I.

Usually, the triangular saw-tooth shape has been realized as a staircase structure in a multilevel diffraction grating [13], [14], but shadowing effects appear [15] when the period is close to the operating wavelength. Traditionally, the manufacture of diffraction gratings has been carried out in two steps. The first step consists of making molds, either with lithography [16] or

by diamond-cutting tools [17]. The second step involves the replication of the profile in polymers or glass. Gray scale e-beam lithographic and etching processes have also been used to draw staircase structures on silicon substrates [18]. Some authors have tested laser ablation techniques to transfer particles from a metallic target to a glass substrate, thus forming the diffraction grating [19]. Reflective diffraction gratings are traditionally made by depositing a metallic coating like gold, aluminum, or silver on an optic substrate and ruling parallel grooves in the surface [20], [21].

However, for space applications, metallic substrates are the most suitable option. Particularly, aluminum alloy 6061T tolerates temperature gradients due to its flat thermal expansion coefficient and high thermal conductivity [22], [23]. This alloy is more resistant to corrosion than 7075 due to the lower amount of copper in its composition and easier to machine [24].

Several grating configurations have been implemented in previous space instruments. For example, two reflective Littrow configuration gratings were used for the field-imaging far-infrared line spectrometer (FIFI LS) for the Stratospheric Observatory for Infrared Astronomy (SOFIA) airborne observatory, operating at first and second orders [25], [26]. Alternatively, the Photoconductor Array Camera and Spectrometer (PACS) instrument [27] on the Herschel space observatory uses a single diffraction grating that covers the entire spectral range (55–210  $\mu\text{m}$ ) and works in the first three orders of diffraction with an efficiency larger than 0.6. In our case, the proposed grating works in a shorter spectral range than PACS and with a single diffraction order. These designs reach efficiency values higher than 90% for the ideal design [10] and, as we will show along this contribution, this figure is greater than 75% for the fabricated gratings.

Table I resumes the initial specifications for the grating given by the spectrometer constraints. The parameters of the diffraction grating profile were optimized considering the fabrication limitations and the fulfillment of the specifications [10]. The experimental diffraction efficiency for all the wavelengths should be over 65% to meet SPICA sensitivity requirements. Another requirement is related to the state of polarization of the light reaching the grating. For a better performance, we have chosen the TM component. Working with this polarization implies utilizing a blazed geometry with a saw-tooth profile, enhancing diffraction efficiency [28]. The design of the spectrometer limits the angle of incidence to  $57^\circ$  and the spectral resolution  $\lambda/\Delta\lambda = 200$ . The resulting designed metallic grating has a period  $d = 76 \mu\text{m}$ , a blaze angle  $\gamma = 23.5^\circ$ , and a slant angle  $\beta = 10^\circ$ . The spectral resolution conditions,  $\lambda/\Delta\lambda$ , implies the illumination of 200 periods for  $m = 1$ , meaning that the illumination spot on the grating should be larger than 15.2 mm along the direction of the period.

### III. MANUFACTURING AND GRATING PROFILE CHARACTERIZATION

Different methods of fabrication of blaze gratings have been proposed, including micromachined [29] or laser fabrication [30]. With the conditions presented in Table I, a metallic diffraction grating made of aluminum was manufactured by

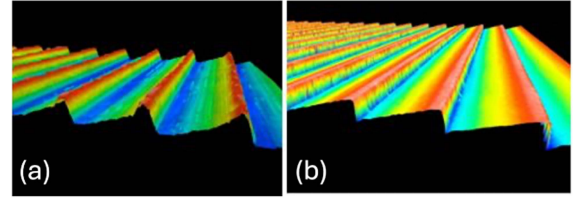


Fig. 2. Topography obtained from confocal microscopy for the grating manufactured using micromachining techniques by (a) milling and (b) femtosecond laser ablation.

the company Arquimea Advanced Systems (Madrid) by micromilling. This is a subtractive manufacturing process that uses a rotating cutting tool to remove material by chip removal. The machine used is a high-performance machining center, brand MIKRON, which uses a 5000–6000-r/min spindle rotating and moves in the three Cartesian axes with millesimal precision while the workpiece remains fixed to the work table. To achieve the desired angle and height, the custom-sharpened tool, with a tip angle of  $67.17^\circ$ , dips 42 microns in each pass. Two passes are made in each direction before moving on to the next profile. The machine is placed on an insulated slab and the external temperature is controlled within a range of  $20 \pm 2^\circ\text{C}$ .

Besides this micromachined fabrication, Microrelleus, S.L. (Barcelona) has engraved a  $4 \times 5 \text{ cm}^2$  grating by high-accuracy laser micromachining with a femtosecond laser system. The laser source used in this fabrication was Satsuma HP3 (Amplitude, Inc, San Francisco, CA, USA) integrated into a five-axis laser center, which emits 250 fs pulses at 1064 nm. The output beam diameter is 0.015 mm with a rounded shape. A 63-mm lens system has been used to focus the beam. The profile of both gratings was measured by confocal microscopy (Confocal Imaging Profiler PL $\mu$ , SENSOFAR). The topographic maps are presented in Fig. 2. These maps reveal that the micromilled profile [see Fig. 2(a)] departs more than the laser-etched [see Fig. 2(b)] from the saw-tooth nominal geometry.

To determine the homogeneity of the profiles over the complete area of the diffraction gratings, the geometry of the engraved saw-tooth profile has been measured on  $2.36 \times 1.98 \text{ mm}^2$  rectangles at nine locations regularly distributed on the gratings (see inset in Fig. 3). For each line that is measured, approximately 30 saw-tooth profiles are obtained. This results in approximately 90 000 characterized profiles in each region, as the scan is generated with 686-nm steps.

Fig. 4 shows two violin plots depicting the statistical distribution of height (top) and period (bottom) across the nine measured regions in the manufactured gratings located at the positions marked in the inset of Fig. 3. These distributions are shown in blue (left) for the diffraction grating manufactured by micromilling and in red (right) for the grating manufactured by laser. Each violin plot includes three dashed lines representing the first quartile, median, and third quartile of each region. The data dispersion is qualitatively indicated by the width of the violin plot, with a greater width corresponding to higher dispersion. For a quantitative analysis, the plot features a solid line that represents the nominal value of  $h$ . The position marked as “mean” shows the mean values and standard deviations of the



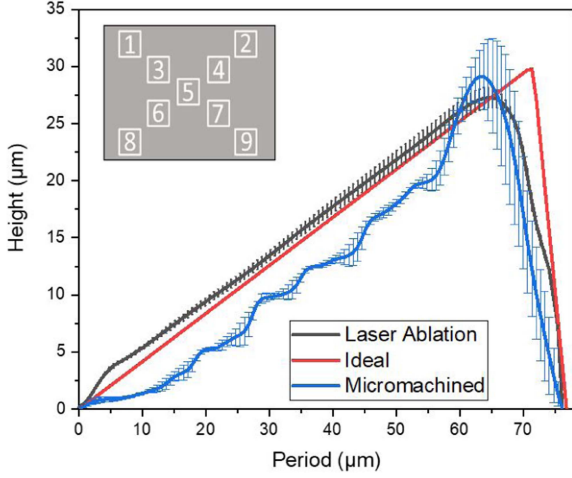


Fig. 3. Saw-tooth ideal profile (red) compared with the measured parameters of the two diffraction gratings. The blue line corresponds to the micromachined grating, while the black line represents the laser-engraved grating. The inset in the figure shows the nine regions along the entire grating where statistical measurements were taken.

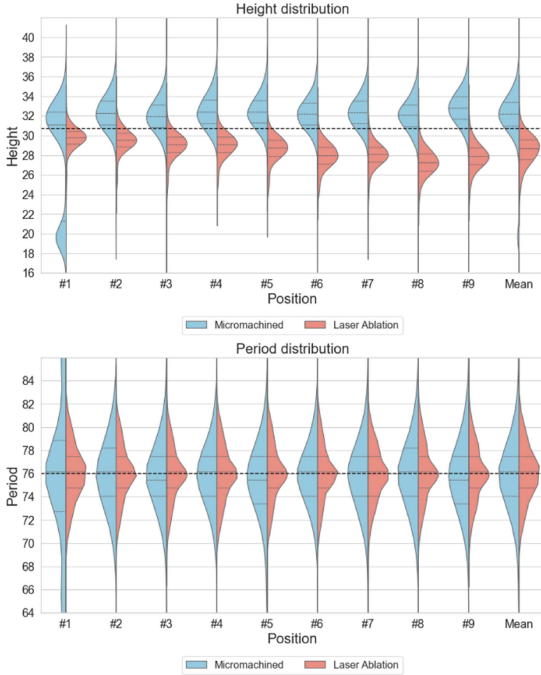


Fig. 4. Height (top) and period (bottom) distributions for the two diffraction gratings plotted on a violin plot in nine different regions plus an additional plot showing the average of all the regions. The blue plot corresponds to the micromachined grating, while the red plot corresponds to the laser-manufactured grating. A dashed line across the graph represents the nominal values of both parameters. Within each violin plot, we have represented three dashed lines: the central line is the median value of each plot, meanwhile the outer lines delimit the first and third quartiles.

entire gratings. The height distribution graph shows that the average of the grating manufactured by micromachined is larger than that of the laser-manufactured grating. In addition, the larger shaded area and greater width of the violin plots indicate greater variability in the profile heights of the micromachined grating. The data distributions in the different regions of both gratings are symmetrical concerning the center of the distributions, except in region #1 of the milled grating, where a concentration of

TABLE II  
MORPHOLOGICAL PARAMETERS OF THE SAW-TOOTH PROFILES

	Ideal Profile	Real Profile Laser Ablated	Real Profile Micromachined
Period, $d$ [ $\mu\text{m}$ ]	76	$76 \pm 3$	$76 \pm 4$
Height, $h$ [ $\mu\text{m}$ ]	30.7	$28 \pm 2$	$31 \pm 3$
Blaze angle, $\gamma$ [ $^\circ$ ]	23.5	$23.1 \pm 0.1$	$26.5 \pm 0.1$
Slant angle $\beta$ [ $^\circ$ ]	10	$18 \pm 1$	$23 \pm 2$

profiles with anomalous heights is observed. The plots of the laser-fabricated grating show that the heights in the regions corresponding to the upper part of the grating (regions 1–4) are higher than in the lower part of the grating (regions 6–9). The laser-engraved surface has a shorter average height than the micromachined grating. In the period distribution plot, as in the case of height, the widths of the violin plots and the standard deviation of the milled grating are larger, indicating greater variability in period values. The interquartile range is smaller for the laser-machined grating than for the micromachined grating. This means that there is less dispersion around the median. For both gratings, the distribution of the period values is similar, except in region #1 of the milled grating. Here, due to manufacturing defects, profiles with periods of smaller dimensions than those designed appear. The two manufacturing methods produce periods of similar dimensions along the complete grating. When comparing both fabrication methods, we find that the laser ablation technique generates profiles with better homogeneity, lower standard deviation, and closer to the nominal values.

When including the variability of the geometrical parameters measured by confocal microscopy, we can add the observed standard deviation to the averaged profiles already shown in Fig. 3. These plots also confirm that the grating fabricated using laser ablation (represented in black) is closer to the ideal profile, meanwhile the micromachined grating has more ripples and larger variations in the profile, which also departs more from the nominal case, especially at the apex of the saw-tooth profile. Table II summarizes these discrepancies between the morphological parameters (height, period, blazed, and slant angles) manufactured gratings and the ideal profile. We can see how both gratings deviate from the designed one, as shown by the distribution of periods and heights and the calculated average profile. In fact, the slant angle  $\beta$  is about twice the nominal value for both gratings. This means that these manufacturing techniques fail to reproduce the peak of the topography, showing a value of the slant angle that should be considered as a limitation of the fabrication and included in the optimization of the design. Therefore, new designs for the ideal profiles should contain slant angles according to this. For the grating produced by micromachined techniques, these deviations are much more pronounced. The dimensions of the laser-ablated grating are close to the design profile. Due to the uniformity of the manufactured profiles, the standard deviation of the measured values is smaller for the laser-manufactured grating than for the micromachined one.

#### IV. SPECTRAL DIFFRACTIVE EFFICIENCY MEASUREMENT

The THz range presents significant challenges for the experimental validation of optical components due to the limited

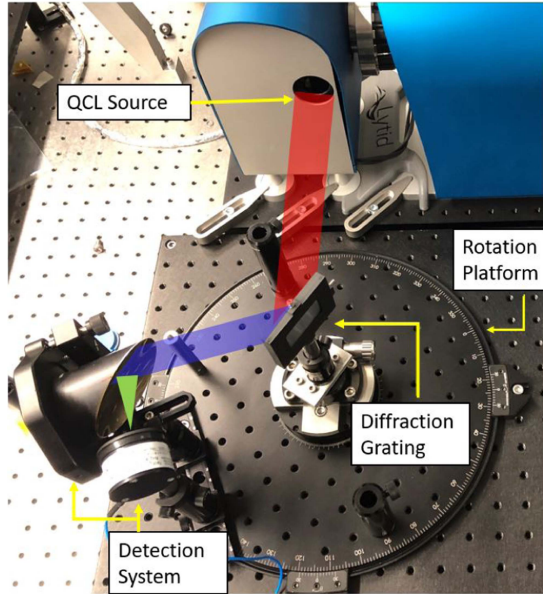


Fig. 5. Experimental setup used to measure the diffraction efficiency of the fabricated gratings. The sample is placed in the center of a goniometer. A polarized and collimated laser beam is directed toward the diffraction grating (red path), the diffracted beam is then collected by the off-axis parabolic mirror (blue path) and focused on the pyroelectric detector (green path). The rotating platform allows the detection system to collect the diffractive orders of interest.

instrumentation available in this spectral region. The scarcity and expense of reliable radiation sources are crucial issues. Our approach has used monochromatic THz sources. Fig. 5 shows the experimental setup. The radiation emission system (TeraCascade 1000, LYTID SA) is based on a state-of-the-art quantum cascade technology and has six chips at selected wavelengths (63.83, 73.17, 76.92, 88.02, 103.5, and 120.0  $\mu\text{m}$ ). The average power output for each band is higher than 1 mW. As far as the diffraction grating was designed to work optimally in the 70–114- $\mu\text{m}$  range, only four of the six laser sources emit within this spectral range. However, we expanded the wavelength range to include all six laser emission sources. While some of the values may not yield good results in the diffraction efficiency, they will serve to validate the simulations and check the reliability of the experimental setup. An automated beam collimator module prepares the 25-mm diameter collimated output beam. The electrically modulated signal was sent to the amplifier. The measurements were taken after a minimum warm-up period of 30 min to achieve a stable signal. A wire grid polarizer (wire of 5- $\mu\text{m}$  diameter and 22- $\mu\text{m}$  wire spacing) (Pure-WavePolarizers Ltd.) allowed us to select the TM component reaching the grating.

The setup is composed of two independent rotating platforms. The outer rotating breadboard has a central aperture to place a goniometer directly on the optical bench which allows the inner goniometer to be fixed while the outer rotating platform moves. The diffraction grating was placed in the inner goniometer on a nonmoving mount with lateral and vertical fixings to ensure its position, so that the radiation from the laser source hits the diffraction grating at the intended angle. The detection system is installed on the outer rotation stage, which, together with the central rotation system, is used to gather the diffractive orders

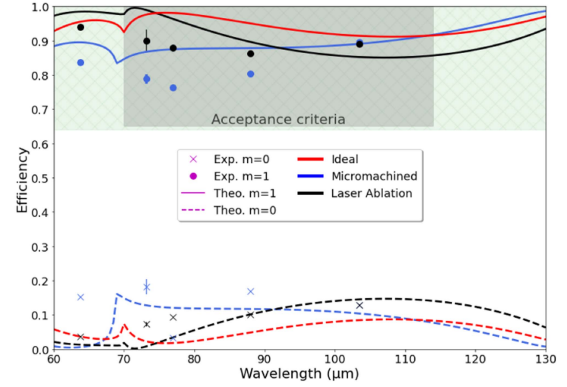


Fig. 6. Diffraction efficiency versus wavelength for the laser engraved grating (black) and the traditionally micromachined grating (blue). The lines in red are for the ideal profile. The solid curves represent the theoretical efficiency of first diffraction order of the profiles. The dashed curve is the theoretical zeroth-order efficiency. The cross and dots represent the maximum diffraction efficiency values of the zeroth and first orders, respectively. The green shaded area represents efficiencies above the 65% threshold set by the system requirements, while the darker shade indicates the wavelength range for which the design was optimized. The experimental values of the efficiency for  $\lambda = 103.5 \mu\text{m}$  coincide, and the symbols overlap.

of interest ( $m = 0, 1$ ). The diffracted beam is focused by a 2" gold-coated off-axis parabolic mirror on a pyroelectric detector (THz 20, Sensor und Lasertechnik). This detector has 20 mm of aperture and a responsivity of 140 V/W at a frequency of 1.4 THz. This detector sends its signal to a current preamplifier. The amplified signal is then read with a lock-in amplifier (Stanford Research Systems, SR830), with a 10-M $\Omega$  input impedance and sensitivity of 2 nV, modulation frequency of 18 Hz and 50% duty cycle.

An additional visible light emitting diode (LED) was used as an illumination source to properly align the setup with the help of another off-axis-parabolic mirror and some viewing screens.

The diffraction efficiency of order  $m$ ,  $\eta_m$ , is the ratio between the optical power contained in that order,  $P_m$ , that propagates away from the grating and the incident optical power  $P_{\text{inc}}$

$$\eta_m = \frac{P_m}{P_{\text{inc}}}. \quad (2)$$

In our experimental setup,  $\eta_m$  is the ratio between two signals acquired by the detector.  $P_m$  is the signal obtained when the detector collects the diffractive order  $m$  at the given diffraction angle,  $\theta_m$  with an angle of incidence  $\theta_{\text{inc}}$ . The denominator in (2),  $P_{\text{inc}}$ , corresponds to the signal obtained with the same geometry but replacing the grating with a reference mirror. Operationally, when the system is adjusted to measure the selected diffraction order, we move the detection arm to obtain read-outs at angles close to the expected diffraction angle. Then, these points are used to fit a Gaussian and obtain the maximum of the signal, that is taken as the detected power of the radiation reflected by the grating at the given order.

A first experimental validation has been made by measuring the efficiencies  $\eta_0$  and  $\eta_1$  when the angle of incidence is set to the nominal value,  $\theta_{\text{inc}} = 57^\circ$  (see Table I). To do that, we took a series of ten measurements for five wavelengths: four inside the spectral range of interest and a fifth one at a shorter wavelength ( $\lambda = 63.83 \mu\text{m}$ ). The results are presented in Fig. 6, where the

shaded region represents the spectral range of interest above the efficiency threshold,  $\eta_{\text{threshold}} = 0.65$ , obtained for  $m = 1$ . In this plot, the black and blue dots are for the measured  $\eta_1$  for the laser-ablated and micromachined gratings, respectively. The error bars corresponding to the standard deviation of the ten different measurements for each frequency are included, although they are only noticeable at the 73-micron wavelength, perhaps due to possible instability of the signal emission of this laser. Fig. 6 also contains the results obtained from simulations based on the measured profiles (in blue for the micromachined grating and in black for the laser-ablated grating), and the calculated efficiencies for the ideal profile (in red). The morphological issues detected in the previous section—large profile irregularity, increased values of the blaze and slant angles, and the presence of a flat surface at the beginning of the profile slope—can result in a significant drop in the diffractive efficiency. This problem was already addressed [10] by calculating the diffractive efficiency of grating having a profile that is the average of the manufactured grating profiles measured by confocal microscopy. In this article, we have followed the same approach using a better dataset obtained from a wider sample analysis. The grating manufactured by laser ablation exhibits higher efficiencies at the first order,  $m = 1$ , at shorter wavelengths, decreasing at longer wavelengths (see solid black line in Fig. 6). On the other hand, the grating manufactured using micromachined (solid blue line in Fig. 6) displays the opposite behavior, with better efficiency at longer wavelengths. This behavior is caused by the departure in the values of the blazed angle  $\gamma$  and the slant angle  $\beta$  from the ideal values (see Table II). In a previous publication [10], we analyzed the dependence of the spectral efficiency in terms of these two angles. This previous study explains the behavior seen in Fig. 6. When the slant angle increases, the maximum of the spectral efficiency blueshifts. At the same time, this maximum moves to longer wavelengths when increasing the blazed angle. Our micromachined grating has larger-than-ideal slant angles. On the other hand, the laser engraved grating has a blazed angle slightly smaller than the ideal one, meanwhile, the micromachined grating shows a blazed angle significantly larger. All this together, helps to understand the spectral behavior of the efficiency shown in Fig. 6. For both fabricated gratings, the simulated efficiency is above 0.8 within the whole spectral range. Although computational electromagnetism is a quite reliable tool to optimize and analyze the design of optical components, their validation always needs an experimental verification of their performance. Then, merging all these findings, it can be concluded that both fabrication approaches generate diffraction gratings with performance above the threshold  $\eta_1 > 0.65$ . However, the experimental results show that the laser-ablation manufacturing produces gratings with better optical performance, in terms of  $\eta_1$  ( $\eta_1 > 0.86$ ), than the micromachined gratings ( $\eta_1 > 0.76$ ).

The availability of the goniometric setup and the lack of a continuously tunable source suggested measuring  $\eta$  in terms of the angle of incidence for the six available wavelengths to obtain more experimental data points. These measurements are useful for better understanding the angular limitations of the gratings and for comparing the experimental results with those obtained from the simulations. The computational

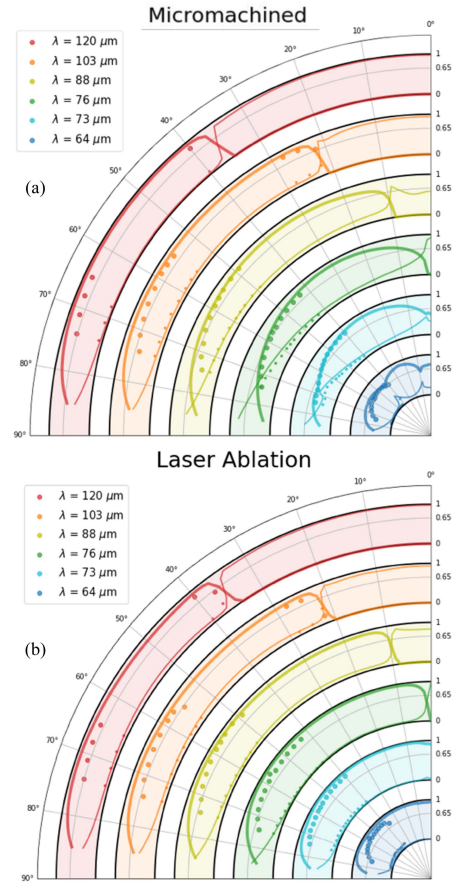


Fig. 7. Polar diagram of the diffraction efficiency versus the angle of incidence,  $\theta_{\text{inc}}$  at six wavelengths for (a) the micromachined grating and (b) the laser ablated grating. Each annulus sector corresponds to a specific wavelength and is represented by a different color. These regions contain the threshold level  $\eta = 0.65$ , to check when the experimental results are above the requirement in efficiency. The angular axis indicates the angle of incidence for each measurement. The thick and thin solid lines represent the simulated efficiency of the first ( $m = 1$ ) and zeroth ( $m = 0$ ) diffraction orders, respectively. These efficiencies have been calculated by modeling measured profiles that are slightly different for each fabrication method. The large and small dots are the measured efficiencies for  $m = 1$  and  $m = 0$ , respectively.

electromagnetism model has been refined to average the response of the grating using profiles from three portions of the gratings: Position #5 (central), Position #1 (superior), and Position #8 (inferior). (See inset in Fig. 3.). Also, instead of using an average profile that is repeated periodically, we have considered a large portion of data by including a profile containing eight periods of the grating extracted from the topographical measurements. (See Fig. 3.). Our model takes these eight periods and generates a supercell that is repeated periodically. The results from simulations for orders  $m = 0, 1$ , along with the experimental values have been represented as polar plots in Figs. 7(a) and (b) for the six wavelengths of incident radiation available at the laboratory and for the micromachined and laser-ablated gratings, respectively. Each section of the polar plot corresponds to one wavelength. Besides the data obtained from the computational electromagnetism package, experimental measures were done to verify the diffraction behavior of the two gratings. To obtain these measurements, the grating was positioned in the mount and set to the angle of incidence using the goniometer. The diffracted



energy was measured at different points around the theoretical diffraction angle, and the maximum value was obtained after a fitting of these measurements with a Gaussian distribution. The measurement at some angles of incidence was forbidden due to the occlusion of the laser beam by the detection system. The polar diagram shows the theoretical diffraction efficiency of the mean profile calculated by the FEM method (colored lines) for 0 and 1 orders versus the experimental values measured for each angle of incidence (dots). The thick lines and large dots are for  $m = 1$ , and the thin lines and small dots are for  $m = 0$ . The experimental measurements are in accordance with the trend predicted by the theoretical ones, but there are discrepancies in the magnitude of the efficiency. The experimental values of  $\eta_1$  are lower than the simulated ones, meanwhile, the differences between measured and simulated efficiencies are smaller for  $\eta_0$ . The simulated results agree better with the experimental data at longer wavelengths, where  $\lambda$  is much larger than the surface irregularities. These irregularities are also responsible for scattering that subtracts power from the angular direction corresponding to the diffractive mode. Despite these differences, experimental measurements show that the laser-made grating is more efficient than the grating micromachined by milling. Besides, the efficiencies for both gratings are above the nominal threshold for a wide angular range, including the operational angle of incidence,  $\theta_{\text{inc}} = 57^\circ$ .

## V. CONCLUSION

The spectrometers for space instrumentation in the THz range use customized diffraction gratings as dispersive elements. Besides the extreme environmental conditions (vacuum, temperature, mechanical vibrations, etc.), due to the spectral and power characteristics of the available observable radiation, these gratings have to perform with the highest possible diffraction efficiency for a given spectral range, a predefined polarization component, and the angle of incidence prescribed by the design. In our case, the grating takes the form of a metallic blazed grating, where the period and saw-tooth parameters have been previously analyzed and set for an optimum design when  $\theta_{\text{inc}} = 57^\circ$ ,  $\lambda \in [70 - 114] \mu\text{m}$ ,  $m = 1$ , and efficiency  $\eta_1 > 0.65$ .

Although computational electromagnetism is a quite convenient tool to study the dependence of the efficiency with the geometrical and material parameters, the actual validation of the elements has to come from experimental measurements. At the same time, the designed geometry has to be transferred to a substrate using the available fabrication tools. We have chosen two techniques: 1) laser ablation; and 2) micromachined to fabricate aluminum blazed gratings with a period  $d = 76 \mu\text{m}$ , and a blazed angle of  $23.5^\circ$ . These gratings have been thoughtfully characterized both morphologically and optically. Confocal microscopy has been used to measure the fabricated topography. From these measurements, we have found that the nominal period has been reproduced quite well with a slightly greater standard deviation for the micromachined ( $d = 76 \pm 4 \mu\text{m}$ ) grating than for the laser-ablated one ( $d = 76 \pm 3 \mu\text{m}$ ). However, the blazed angle is much larger for the micromachined version, with the slant angle below the intended design for both fabrications types. Also, when plotting the average profile, we have seen

how the laser-ablation fabrication provides profiles closer to the nominal one, meanwhile, micromachined gratings show strong discrepancies in the form of microgrooves. In both geometries, the apex of the saw-tooth profiles has been poorly reproduced. The morphological characterization has been used to refine the computational model and include actual topographies from various regions on the grating. Then, the spectral and angular efficiency evaluations have been recalculated.

Moreover, our fabricated gratings have been experimentally tested for six wavelengths in the THz region. The measurement setup has been adapted to obtain reliable values of the efficiencies for the zero and first orders of diffraction. These measurements have been compared to the simulated results in two cases of interest. In the first one, we have fixed the angle of incidence and obtained the efficiency for the five wavelengths available for this configuration. Four of them fall within the range of interest of the spatial spectrometer where these gratings have to be implemented. The results show that the measured efficiencies are well above the threshold  $\eta_1 = 0.65$ . The second round of measurements fixed the wavelength and measured the efficiency in terms of the angle of incidence for the available range of the goniometer. This range has encountered some forbidden intervals where the optical setup at the detection arm is obscured by the laser source. The experimental results have also been compared with the simulated ones. The comparison shows that, for most of the angular range, the efficiency is above the threshold. Also, these data help to understand the limits to mimic the experiment using our computational tools. As it happened with the morphological characterization, we have found that the laser-ablated grating behaves better, with higher efficiency, than the micromachined element. This better performance can be directly related to the close resemblance, except for the slant angle (see Table II), of the laser engraved grating to the ideal topography. The discrepancies between measurement and simulation may be due to scattering from the microgrooves and the deviation from the nominal saw-tooth profile at the apex. As a consequence, we have seen how the slant angle  $\beta$  of the fabricated gratings, is about twice the ideal value. This discrepancy appeared for both manufacturing techniques. Therefore, it could be considered as a fabrication constraint that should be included in the optimization process.

In summary, we have numerically and experimentally validated two aluminum blazed gratings to perform above requirements as dispersive elements in a THz spectrometer for space instrumentation. Laser ablation produces superior gratings both morphologically and optically,  $\eta_1 > 0.86$ , meaning that this fabrication tool should be chosen for the fabrication of high-quality gratings.

## ACKNOWLEDGMENT

The experimental measurements in the THz were made at the Applied Physics Department of the University of Salamanca (USAL) with the help and assistance of Jesús Enrique Velázquez Pérez and Yahya Moubarak Meziani. This collaboration was possible under the framework of the agreement between USAL and INTA for cooperation in scientific research and technical activities.

## REFERENCES

- [1] M. G. Hauser and E. Dwek, "The cosmic infrared background: Measurements and implications," *Annu. Rev. Astron. Astrophys.*, vol. 39, no. 1, pp. 249–307, 2001. [Online]. Available: <https://doi.org/10.1146/annurev.astro.39.1.249>
- [2] H. Dole et al., "The cosmic infrared background resolved by spitzer," *Astron. Astrophys.*, vol. 251, no. 2, pp. 417–429, 2006.
- [3] F. Salama, "Pahs in astronomy—A review," in *Proc. Int. Astron. Union IAU Symp.*, vol. 251, 2008, pp. 357–366.
- [4] P. R. Roelfsema et al., "Spica—A large cryogenic infrared space telescope: Unveiling the obscured universe," *Publ. Astron. Soc. Aust.*, vol. 35, 2018, Art. no. e030.
- [5] D. Arrazola et al., "The optical design of a far infrared spectrometer for spica: Grating modules evaluation," *Soc. Photo-Opt. Instrum. Engineers*, vol. 10708, Jul. 2018, Art. no. 107083.
- [6] D. Farrah et al., "Review: Far-infrared instrumentation and technological development for the next decade," *J. Astron. Telescopes, Instruments, Syst.*, vol. 5, no. 2, 2019, Art. no. 020901. [Online]. Available: <https://doi.org/10.1117/1.JATIS.5.2.020901>
- [7] G. Chin et al., "Single aperture large telescope for universe studies (SALTUS): Science overview," 2024, *arXiv:2405.12829*.
- [8] L. Bisigello et al., "Disentangling the co-evolution of galaxies and supermassive black holes with prima," *Astron. Astrophys.*, vol. 689, 2024, Art. no. A125. [Online]. Available: <https://arxiv.org/pdf/2404.17634>
- [9] M. A. Golub and A. A. Friesem, "Analytic design and solutions for resonance domain diffractive optical elements," *J. Opt. Soc. Am A*, vol. 24, no. 3, pp. 687–695, Mar. 2007. [Online]. Available: <https://opg.optica.org/josaa/abstract.cfm?URI=josaa-24-3-687>
- [10] A. Cuadrado et al., "Diffraction efficiency of reflective metallic gratings operating in the THz range," *IEEE Trans. THz Sci. Technol.*, vol. 13, no. 6, pp. 605–613, Nov. 2023. [Online]. Available: <https://ieeexplore.ieee.org/document/10258338>
- [11] M. G. Moharam and T. K. Gaylord, "Rigorous coupled-wave analysis of metallic surface-relief gratings," *J. Opt. Soc. Am A*, vol. 3, no. 11, pp. 1780–1787, Nov. 1986. [Online]. Available: <https://opg.optica.org/josaa/abstract.cfm?URI=josaa-3-11-1780>
- [12] C. Multiphysics, "Comsol multiphysics," <https://www.comsol.com/>, [Accessed 2023]. [Online]. Available: <https://www.comsol.com/>
- [13] M. B. Fleming and M. C. Hutley, "Blazed diffractive optics," *Appl. Opt.*, vol. 36, no. 20, pp. 4635–4643, 1997.
- [14] T. J. Suleski, *Diffractive Optics: Fabrication*. Boca Raton, FL, USA: CRC Press, 2015.
- [15] O. Sandfuchs, R. Brunner, D. Pätz, S. Sinzinger, and J. Ruoff, "Rigorous analysis of shadowing effects in blazed transmission gratings," *Opt. Lett.*, vol. 31, no. 24, pp. 3638–3640, Dec. 2006. [Online]. Available: <https://opg.optica.org/ol/abstract.cfm?URI=ol-31-24-3638>
- [16] S. Tj and O' Shea, "Gray-scale masks for diffractive-optics fabrication: I commercial slide imagers," *Appl. Opt.*, vol. 34(32), no. 10, pp. 7507–7507, Nov. 1995. [Online]. Available: <https://pubmed.ncbi.nlm.nih.gov/21060625/>
- [17] L. Li et al., "Fabrication of diffractive optics by use of slow tool servo diamond turning process," *Opt. Eng.*, vol. 45, no. 11, 2006, Art. no. 113401. [Online]. Available: <https://doi.org/10.1117/1.2387142>
- [18] J. Kim, D. Joy, and S.-Y. Lee, "Controlling resist thickness and etch depth for fabrication of 3D structures in electron-beam grayscale lithography," *Microelectron Eng.*, vol. 84, no. 12, pp. 2859–2864, 2007. [Online]. Available: <https://www.sciencedirect.com/science/article/pii/S0167931707003164>
- [19] A. I. Gómez-Varela, A. Castelo, C. Gómez-Reino, X. F. de la Fuente, and M. T. Flores-Arias, "Diffractive gratings fabrication on glass with a laser Nd:YVO<sub>4</sub>," *Optica Pura Aplicada*, vol. 43, no. 2, pp. 95–99, 2010. [Online]. Available: <https://digital.csic.es/bitstream/10261/47984/1/Fabricaci%C3%B3n%20de%20redes.pdf>
- [20] R. Paschotta, "Diffraction gratings," RP Photonics Encyclopedia. [Online]. Available: [https://www.rp-photonics.com/diffraction\\_gratings.html](https://www.rp-photonics.com/diffraction_gratings.html)
- [21] [Online]. Available: [https://www.thorlabs.com/navigation.cfm?guide\\_id=9](https://www.thorlabs.com/navigation.cfm?guide_id=9)
- [22] [Online]. Available: [https://amesweb.info/Materials/Thermal\\_Expansion\\_Coefficient\\_of\\_Aluminum.aspx#google\\_vignette](https://amesweb.info/Materials/Thermal_Expansion_Coefficient_of_Aluminum.aspx#google_vignette)
- [23] [Online]. Available: <https://industrialmetalservice.com/metal-university/aluminum-6061-material-properties/>
- [24] [Online]. Available: <https://leadrp.net/es/blog/aluminum-6061-vs-7075-which-one-is-right-for-you/>
- [25] W. Raab et al., "Characterizing the system performance of FIFI LS: The field-imaging far-infrared line spectrometer for SOFIA," in *Proc. Ground-Based Airborne Instrum. Astron.*, I. S. McLean and M. Iye Eds., vol. 6269, 2006, Art. no. 62691G. [Online]. Available: <https://doi.org/10.1117/12.671483>
- [26] M. Schweitzer et al., "Verification of the optical system performance of fifi-ls: The field-imaging farinfrared line spectrometer for Sofia," *Proc. SPIE*, vol. 7014, 2006, Art. no. 70140Z.
- [27] A. Poglitsch et al., "The photodetector array camera and spectrometer (pacs) on the herschel space observatory\*," *Astron. Astrophys.*, vol. 518, 2010, Art. no. L2. [Online]. Available: <https://doi.org/10.1051/0004-6361/201014535>
- [28] G. Sridharan, V. Pramitha, and S. Bhattacharya, "Design and fabrication of lower aspect ratio sub-wavelength grating for polarization separation," in *Proc. Int. Conf. Fibre Opt. Photon.*, Optica Publishing Group, 2012, Art. no. MPO.14. [Online]. Available: <https://opg.optica.org/abstract.cfm?URI=Photonics-2012-MPO.14>
- [29] J. Gao, P. Chen, L. Wu, B. Yu, and L. Qian, "A review on fabrication of blazed gratings," *J. Phys. D: Appl. Phys.*, vol. 54, no. 31, 2021, Art. no. 313001.
- [30] J. Fantova et al., "Single-step fabrication of highly tunable blazed gratings using triangular-shaped femtosecond laser pulses," *Micromachines*, vol. 15, no. 6, 2024, Art. no. 711.



**Gonzalo García-Lozano** was born in 1988, in Madrid, Spain. He received the master's degree in optical and imaging technologies from the Complutense University of Madrid, in 2020. He is currently working toward the Ph.D. degree in optical design and integration with the Department of Space Optics, Instituto Nacional de Técnica Aeroespacial, Madrid, Spain.

His research interests include developing instrumentation for space exploration in the Terahertz range, including Far-IR Optics, Diffraction Gratings, and Quasi-optical systems.



**Guillermo Mercant** was born in Madrid in 1993. He received the degree in physics from the Complutense University of Madrid, Madrid, Spain, and the master's degree in data science from the International University of Valencia, Valencia, Spain.

For two years he has been on a training fellowship with Space Optics Department, Instituto Nacional de Técnica Aeroespacial, Madrid, researching quasi-optical systems, far infrared optics and spectrometers. He is currently an AIT Engineer with the Astrobiology Center, Consejo Superior de Investigaciones Científicas, Madrid, for the HARMONI instrument of the ELT, and working with machine learning models for space flight models.



**Marianela Fernández-Rodríguez** received the Ph.D. degree in physics (optics) from the Universidad Autónoma de Madrid, Madrid, Spain, in 2015.

She has participated in national and international projects, all of them within the space sector, such as the European Space Agency's ExoMars mission for the exploration of Mars, missions for the exploration of deep space, or in Earth observation satellite. She has also collaborated in research projects, such as "Characterization of Optical Materials for Space,"

"Thermoluminescence study of color centers induced by gamma radiation in optical materials in space application" or for the development of absorbent layers and nanophotonic structures for the development and optimization of optical devices. She is currently an Optical Engineer with the Department of Space Optics, National Institute of Aerospace Technology, Madrid. Her research interests include the optical design and integration of space instrumentation, the characterization of optical materials for space applications, and optical analysis technique ellipsometry spectroscopic.





**María Carmen Torquemada** received the M.Sc. degree in physics, specialty in materials physics, and the Ph.D. degree in physics from the Complutense University of Madrid, Madrid, Spain, in 1990 and 1994, respectively.

During her Ph.D., she worked on surface physics and the reactivity of gases on surfaces under ultra-high vacuum conditions, with the Institute of Materials Science, Consejo Superior de Investigaciones Científicas, Madrid. From 1966 to 2015, she was a scientific Researcher with the Navy Research and Development Center, Madrid. Her primary work focused on developing and processing polycrystalline infrared PbSe smart detectors and their applications in defense. In 2015, she joined the Space Optics Department, Instituto Nacional de Técnica Aeroespacial, Madrid. Her main tasks include the development of space instrumentation and the characterization of materials. Her research interests include smart sensors, terahertz radiation, far-IR optics, spectrometers, diffraction gratings, optical coatings, nanoparticles, surface science, scanning electron microscopy, atomic force microscopy, and X-ray microanalysis.



**Luis M. González** received the Ph.D. degree in physics (optics) from the Complutense University of Madrid, Madrid, Spain, in 2009.

He is currently an Optical Engineer and Head of Optical Design and Integration with the Space Optics Department, Instituto Nacional de Técnica Aeroespacial (INTA), Madrid, where he has developed most of his career in optical engineering. He has more than 30 years of experience in optics, 26 of them in the field of space optics. He has participated in the development of optical payloads for space projects, Earth observa-

tion and scientific missions, assuming responsibilities in design and integration. He is responsible for the Space Optics Integration & Test Laboratories, INTA. He is also a Research Scientist. He has authored or coauthored of more than 25 papers in the field of optics. His research interests include applied optics in the areas of optical modeling and free-form optics.



**Tomás Belenguer** received the degree in physics (optics) from the University of Zaragoza, Zaragoza, Spain, and the Ph.D. degree in physics from the Complutense University of Madrid (UCM), Madrid, Spain.

He has been a member of the technical staff, Instituto Nacional de Técnica Aeroespacial (INTA), Madrid, since 1995. He has developed his professional career in optical engineering applied to industrial and space optical systems and equipment. He has more than 30 years of experience in design,

integration, and characterization of optical instrumentation and more than 20 years of experience in space programs. Since 2009, he has been the Head of LINES (Laboratory of Space Instrumentation), Consejo Superior de Investigaciones Científicas, Madrid, and responsible for coordinating teamwork in the optomechanical design of instrumentation. He is currently the Head of the Space Optics Department, INTA. He has supervised three doctoral theses and has four in preparation. He has coordinated more than 12 master's theses in the optics faculty of the UCM. He has authored or coauthored more than 100 publications in optical research and optical instrumentation techniques.



**Alexander Cuadrado** received the graduation degree in electronic engineering from the Euskal Herriko Unibertsitatea, Bilbao, Spain, in 2010, the M.S. degree in photonics from the Universidad Autónoma de Madrid, Madrid, Spain, in 2011, and the Ph.D. degree in optics from the University Complutense of Madrid, Madrid, in 2014.

He was a Postdoc with the Institute Daza de Valdés, Spanish National Research Council, Universidad Autónoma de San Luis Potosí and Universidad Complutense de Madrid. He is currently an Associate

Professor of Electronic Technology with Universidad Rey Juan Carlos de Madrid, Madrid. His research interests include the wide area of nanophotonic, with special emphasis in nanoantennas, metamaterials, nonconventional materials, diffraction, and solar cells.

Dr. Cuadrado was the recipient of the Universidad Complutense de Madrid Excellency Award.



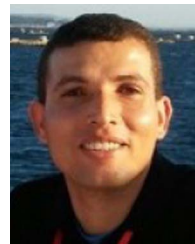
**Luis Miguel Sánchez-Brea** received the B.Sc. and Ph.D. degrees in physics from the Complutense University of Madrid, Madrid, Spain, in 1995 and 2001, respectively.

He is currently an Associate Professor with the Optics Department, Complutense University of Madrid. He lectures on Physical Optics and Digital Optics. He has also been R&D technician with Fagor Automation S. Coop. and Ramón y Cajal Researcher. He has been a Secretary and Head of the Optics Department, and directed the master's degree in new electronic and photonic technologies. He has also supervised three doctoral thesis and 28 master's thesis. He has authored or coauthored more than 100 publications. His research interests include diffraction, diffractive optical elements, polarization, and applied optics.



**Javier Alda** received the degree in science from the Faculty of Science, University of Zaragoza, Zaragoza, Spain, in 1985, and the Ph.D. degree in physics from the University Complutense of Madrid, Madrid, Spain, in 1988.

Since 2010, he has been a Full Professor of Optics. He is currently the Director of Applied Optics, Complutense Group, Madrid. His research interests include the design and analysis of resonant subwavelength structures and their integration with energy harvesting systems, optical sensors, diffractive optics design, and the application of optical engineering solutions to the industry.



**Mahmoud Elshorbagy** received the bachelor's of science degree in physics and the master's of science degree in hybrid solar cells from the Physics Department of the Faculty of Science, Minia University, El-Minya, Egypt, in 2007 and 2013, respectively. He received the Ph.D. degree in physics from the Faculty of Physics, Universidad Complutense de Madrid, Madrid, Spain, in 2020.

He was a Researcher with the Escuela Politécnica Superior of the Universidad Alcalá de Henares, Madrid, and a Fellow of the Applied Optics Com-

plutense Group, Universidad Complutense de Madrid, Madrid. He was previously a Fellow of the Displays and Photonic Applications Group, Universidad Carlos III de Madrid, Getafe, Spain. From 2021 to 2022, he held a Postdoctoral position with the Faculty of Physics, Universidad Complutense de Madrid, where he is currently a Visiting Professor with the Faculty of Optics and Optometry. His research interests encompass the development of efficient photonic devices utilizing resonant nanostructures and advanced light concentration strategies. His research also involves diffractive optics, energy harvesting, sensing devices, nanofabrication, and computational electromagnetism.